

# Symmetries at the Anderson transition of correlated two-dimensional electrons

Mathieu Lizée,<sup>1,2,\*</sup> Mohammadmehdi Torzadeh,<sup>2</sup> François  
Debontridder,<sup>2</sup> Marie Hervé,<sup>2</sup> Christophe Brun,<sup>2</sup> and Tristan Cren<sup>2,†</sup>

<sup>1</sup>*Laboratoire de Physique de l'École Normale Supérieure - ENS Université PSL - Paris France*

<sup>2</sup>*Sorbonne Université - CNRS - Institut des NanoSciences de Paris - France*

The interplay of Anderson localization with Coulomb repulsion shows deep links with superconductivity [1, 2] and with the many-body localization of quantum systems [3]. Here, we map the electronic states of a tin monolayer known for its Mott and antiferromagnetic behavior [4–6] across its metal-insulator transition close to a band-edge. Using spatial correlations of local density of states (LDOS), we clearly identify the mobility edge and its critical exponent of  $\nu = 0.75 \pm 0.1$ . We observe that LDOS distribution functions on one hand and multifractal spectra on the other, obey two exact symmetry relations rooted in the Weyl group symmetry of non-linear  $\sigma$ -models [7–9]. In agreement with theoretical predictions, these relations hold all the way from extended to strongly localized states. We also report a power-law scaling of LDOS fluctuations close to the gap-edge  $|E - E_{\text{edge}}|^{-1.7}$  deep in the localized regime. Using tight-binding models, we show that breaking time-reversal symmetry improves the agreement with experiments over the standard Anderson model for our Mott-type system. Overall, we build a unifying picture of localization at the gap-edge of a strongly correlated 2d material and show that localization patterns informs on the underlying symmetry class of disordered electronic systems.

The combined role of disorder and electronic interactions is crucial in the context of low-dimension superconductivity where the multifractality of wave functions close to the localization transition is believed to enhance the critical temperature  $T_c$  [1, 10, 11]. Strikingly at odds with the usual quantum criticality picture, recent kinetic inductance measurements in indium-oxide films hint at a first-order transition from a superconductor to a Bose glass [12]. In normal metals on the other hand, the interplay of Coulomb repulsion with disorder yields the Mott-Anderson transition [13]: in 2D systems, the Coulomb repulsion is predicted to hinder localization, rendering metallic an otherwise localized phase [14]. The possibility of non-trivial topology in a strongly disordered band insulator – the so-called topological Anderson insulator – remains an open question [15].

An original way to probe exotic electronic systems is to study disorder-induced electronic fluctuations. The Anderson transitions were initially classified according to time-reversal and spin-rotation symmetries into the unitary, symplectic and orthogonal classes, corresponding to the Wigner-Dyson classification of the random matrices ensembles. Later, chiral and particule-hole symmetries – which describe respectively hopping in disordered bipartite lattices and superconductors – have broadened the classification. Theoretically, scaling properties and wavefunctions statistics are known for many symmetry classes and dimensions and a number of them has been verified numerically [16]. Thus, we propose to use fluctuations in conductance or local density of states (LDOS) to probe the underlying symmetries of exotic electronic phases.

In recent years, tunneling density of state maps have revealed critical scalings and fractal-like structures in the quantum Hall effect regime [17], at the surface of a 3d magnetic oxide [18] and close to the band edges of epitaxial semiconductors [19–21]. In the superconducting regime, a granularity of the gap width order parameter was observed in relatively strongly disordered thin films [10, 22–24]. In this regime, an enhancement of the superconducting critical temperature  $T_c$  by the multifractality of localized electronic wavefunctions was predicted [1, 11, 25]. At lower disorder, enhanced fluctuations of LDOS close to coherence peaks were observed [26–29] and rationalized as a real-space analog of universal conductance fluctuations [29]. These high spectral resolution tunneling maps provide unmatched insights on the role of disorder in low-dimensional electronic systems.

Due to its 2D nature and to the closeness in energy of exchange interaction and on-site Coulomb repulsion, the  $\sqrt{3} \times \sqrt{3}$  reconstruction of tin on silicon hosts very rich electronic phases. At 77K, a transfer of spectral weight from the Fermi level to two Hubbard bands, as well as the appearance of a quasiparticle peak, shows its Mott insulating behavior [5]. Because of its triangular lattice, it could realize the spin 1/2 triangular antiferromagnetic Heisenberg model which hosts quantum spin liquids and chiral spin states. A possibly chiral superconductivity with a first hint of edge channels was recently observed in the p-doped monolayer [30].

In this study, we investigate the  $\sqrt{3} \times \sqrt{3}$  reconstruction of tin on silicon with high-resolution Scanning Tunneling Spectroscopy (STS). We find the mobility edge using spatial correlation functions – along with the critical exponent  $\nu = 0.75$  – and measure energy-dependent multifractal scalings across the metal-insulator transition. Then, we demonstrate symmetry relations of both LDOS distributions and multifractal spectra predicted from non-

\* lizee@fhi-berlin.mpg.de; Current address: Fritz Haber Institute of the Max Planck Society, Berlin, Germany

† tristan.cren@sorbonne-universite.fr

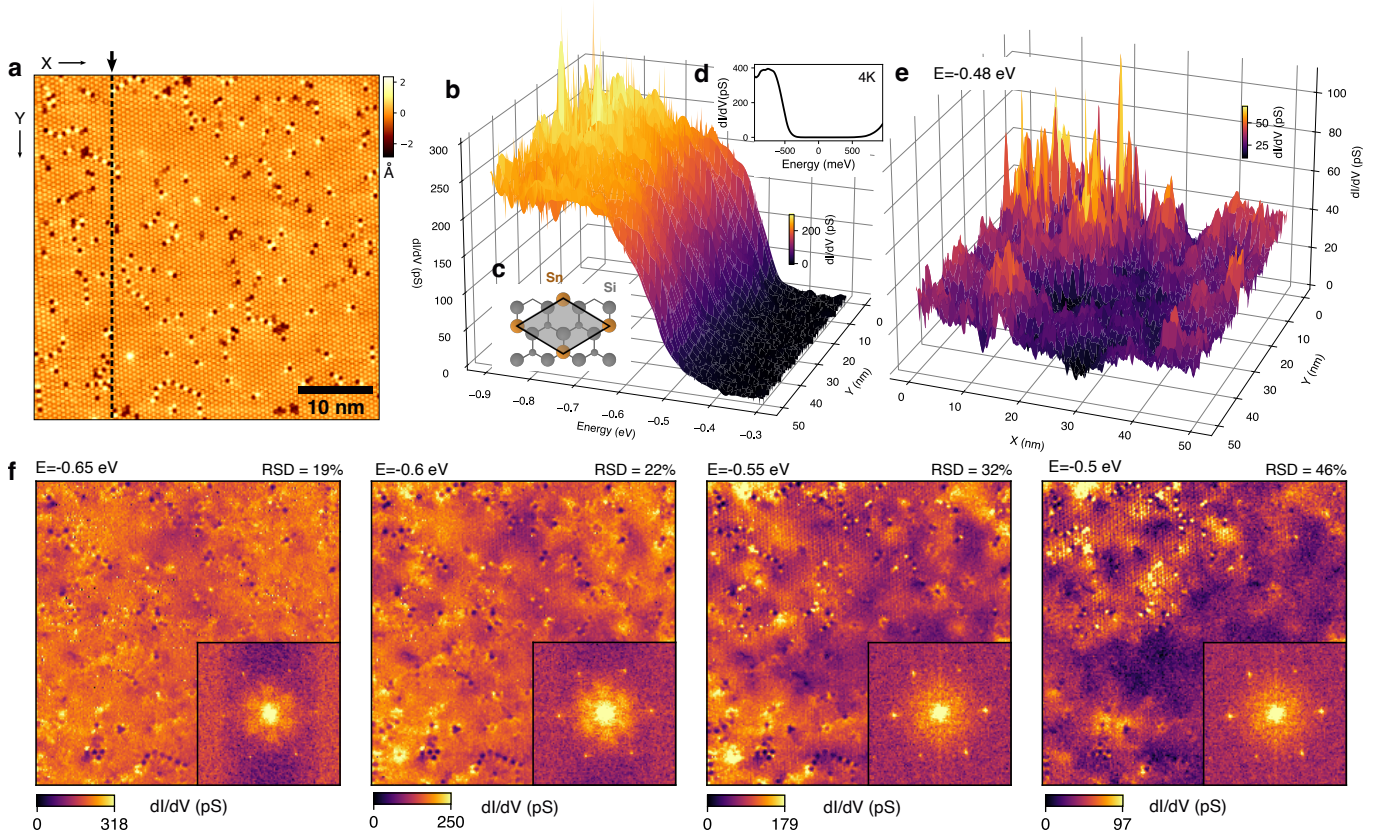


FIG. 1. **a** Topographic map of the tin monolayer deposited on silicon. **b**  $dI/dV$  spectra taken at the lower band-edge of the tin monolayer along a vertical line (cf. the black arrow indicates the X position on **a**). **c** Crystalline structure of the tin  $\sqrt{3} \times \sqrt{3}$  tin reconstruction on a Si(111) surface. **d**  $dI/dV$  spectroscopy at 4K reveals a large gap of roughly 1 eV. **e**  $dI/dV$  map at -480 meV, very close to the band-edge. **f**  $dI/dV$  maps at fixed energy at  $E = \{-0.65, -0.6, -0.55, -0.5\}$  eV along with their Fourier transform.

linear  $\sigma$  models [7–9]. Finally, we show a scaling behavior close to the band-edge in experiments and tight-binding models alike. Strong Coulomb repulsion being expected to drive our system out of the ordinary orthogonal symmetry class, we break time-reversal symmetry with a random magnetic field in the Anderson model and find an improved agreement with experiments.

Overall, our results highlight how the structure of localized states near a band edge reveal the interplay between disorder, Coulomb interactions, and intrinsic electronic symmetries in a model 2D correlated phase. Our approach could be applied to transport coefficients which also show multifractal statistics (see for instance Ref.[31] for graphene) and thus applied to any mesoscopic circuit.

## RESULTS

We prepared the  $\sqrt{3} \times \sqrt{3}$  reconstruction of tin on silicon (111) following the standard recipe [4, 32]: a highly n-doped Si(111) sample with room-temperature resistivity in the  $m\Omega\cdot\text{cm}$  range was flashed to  $1100^\circ\text{C}$  in ultra-high vacuum and slowly cooled down to  $600^\circ\text{C}$  until the

$7 \times 7$  reconstruction was consistently observed. Keeping the substrate’s temperature at  $600^\circ\text{C}$ , we then evaporated  $1/3$  monolayer of tin from an e-beam evaporator (at a rate of about 0.15 monolayer per min) before cooling down the sample to  $500^\circ\text{C}$  in one minute. This procedure yields an almost pure  $\sqrt{3} \times \sqrt{3}$  reconstruction of tin on silicon (111) with domains larger than 100 nm and roughly 3 % of Si-substitutional and Sn-vacancy defects (see Figure 1a). We also report small domains of the denser  $2\sqrt{3} \times 2\sqrt{3}$  phase, in agreement with previous studies [33] – see Supplementary Informations (SI).

Now, focusing on the ground state, we measure tunneling spectroscopic maps at 300 mK across the edge of the conduction band ( $[-1, -0.3]$  V), see the line cut in Figure 1b. The tunneling spectrum at 4 K (Figure 1d) reveals a clear insulating behavior with a large gap between -400 and +500 meV. Spin-resolved ARPES measurements [34] and hybrid-functionals DFT calculations [6] show that this gap corresponds to a row-wise antiferromagnetic ground state and is due to a subtle interplay of strong on-site Coulomb repulsion and exchange interactions. These strong correlations are further confirmed by the Mott insulator signatures observed at higher tem-

perature (77 K) [5].

Deep in the conduction band (Figure 1 **e-f**), we observe delocalized 'metallic' like states, hereafter called metallic, with relatively low dispersion around the mean value (relative standard deviation (RSD) of 19% at  $-0.65$  eV). Close to the gap-edge on the other hand, the density of states is extremely inhomogeneous and concentrates in small regions of the sample whose shape is uncorrelated with the disorder's distribution, a clear hallmark of Anderson localization (RSD of 46% at  $-0.5$  eV). The Fourier transform of the conductance maps of these states show neat Bragg peaks of the  $\sqrt{3} \times \sqrt{3}$  reconstruction. At lower energies, deep into the conduction band, a well developed quasiparticle interference (QPI) signal reflects the band structure of the material and shows the delocalized nature of these electronic states. By contrast, when approaching the band edge, the QPIs become fuzzy while states appear increasingly localized in the real space. A detailed analysis of these QPI patterns will be published elsewhere [6].

## METAL – MOTT-INSULATOR TRANSITION

Critical scalings of LDOS distributions close to metal-insulator transitions were previously reported at the surface of a disordered magnetic insulator [18] and at the band edge of a monolayer transition-metal dichalcogenides [21]. On the theoretical side, a power-law decay of LDOS correlations is expected close to the metal-insulator transition [14]. Let us then plot the angle-averaged 2-point correlation function of  $\eta = dI/dV$  on Figure 2 **a-b**:

$$C(E, R) = \frac{\langle \eta(E, r)\eta(E, R+r) \rangle_r}{\langle \eta(E) \rangle^2} \quad (1)$$

where  $\langle \rangle_r$  denotes spatial averaging. On the  $C(E, R)$  map (see **a**), we show a clear transition between extended and localized states at a critical energy  $E_c = -0.65$  eV which we identify as the mobility edge. The black dashed line follows a power law  $|E - E_c|^{-\nu}$  from which we identify a critical exponent  $\nu = 0.75 \pm 0.1$ . Let us recall that a 2D system in the orthogonal symmetry class has no extended states, merely a diverging localization length at low disorder. Here, Coulomb repulsion could drive the system to the symplectic class where extended states are possible turning  $E_c$  into a fully legitimate mobility edge, but we cannot prove it. Although, the truly extended character of states below  $E_c$  remains uncertain, we still use the concepts of 'extended states' and 'mobility edge' in the following, since *at the scale of our STM map*, they make perfect sense.

On panel **b**, we observe that the decay of correlations with distance is compatible with a power-law close to the band-edge as pointed by the black and red lines that have respective exponents  $-0.03$  and  $-0.1$ . Following Ref [14], we expect  $C(E, R) \sim (L_{Th}/R)^{-\Delta_2}$  as soon as  $R$  is in the diffusive regime, *i.e.*  $\ell < R < L_{Th}$  where

the Thouless length  $L_{Th}$  – which limits diffusion – is the minimum of the system size  $L$ , the localization length  $\xi$  and the inelastic scattering length  $L_\Phi$ . From the critical scalings reported on Figure 2**a-b**, we find the exponent to remain between 0 and  $-0.1$ . Interestingly,  $\Delta_2$  can be obtained independently, using the multifractal analysis of LDOS maps (see panel **c**), as was previously reported on a handful of systems [18, 19, 21, 27, 35].

Here we extract the fractal dimension  $D_2$  – note that  $\Delta_2 = D_2 - 2$  – and the multifractal spectra  $f(\alpha)$  (inset) [36, 37] and report a continuous drop of  $D_2$  when going from non-fractal metallic states below  $E = -0.65$  eV towards multifractal localized states. We find that the power law of spatial correlations matches very closely the multifractal exponent  $\Delta_2$ , not only at criticality but on the entire energy range (see Figure S2), in good agreement with theoretical prediction. Very close to previous measurements on MoS<sub>2</sub> [21] ( $\Delta_2 = -2.28 \times 10^{-3}$ ), we find  $\Delta_2 = -3.3 \times 10^{-3}$  at the mobility edge  $E_c = -0.65$  eV.

## FRACTALITY AND DISTRIBUTION FUNCTIONS

Let us now turn to the full distribution of tunneling conductance values  $P(\tilde{\eta})$  where  $\tilde{\eta} = \eta/\langle \eta \rangle$  at various energies. At weak disorder, all moments of the distribution are given by the second moment  $\sigma(E)$ , in both theory and experiments [28, 29]. The full distribution can thus be computed theoretically and is found to have a log-normal form parametrized by  $\sigma(E)$ . On Figure 3**a**, we plot the distribution functions  $P(\tilde{\eta})$  of the normalized differential conductance  $dI/dV$  at various energies (solid line). We see that the LDOS distributions are continuously broadened when approaching the band edge. Notably, this broadening is very asymmetric and the distribution's fat-tail is strengthened when approaching the band-edge.

A key prediction of non-linear  $\sigma$ -models is a set of exact relations which constrain LDOS distributions and multifractal spectra stemming from the symmetries of the electronic Hamiltonian [9, 38]. In 1994, Mildenberg and Evers have derived a symmetry relation for the distribution function of the normalized LDOS  $\tilde{\rho} = \rho/\langle \rho \rangle$  at criticality [7, 39]

$$P(\tilde{\rho}) = \tilde{\rho}^3 P(\tilde{\rho}^{-1}) \quad (2)$$

An analog relation was found for the multifractal spectra [8]:

$$f(\alpha) = f(2d - \alpha) - d + \alpha \quad (3)$$

Later, relations (2) and (3) were shown to hold due to the Weyl-group symmetry of  $\sigma$ -models by Gruzberg et al., thus removing the condition of criticality [9]. Both relations are thus believed to hold very generally, on both the metallic and insulating sides of the Anderson transition.

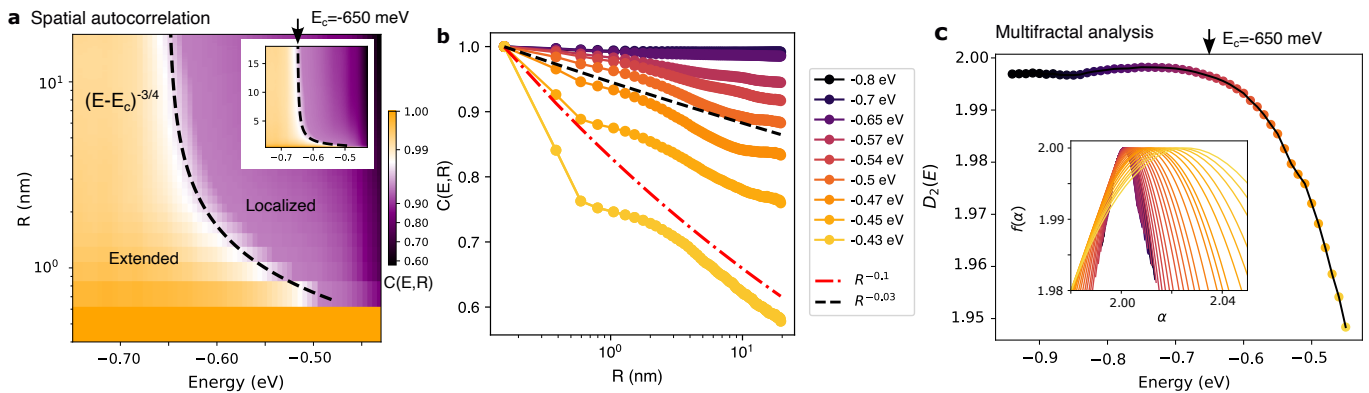


FIG. 2. **LDOS correlation functions** **a** Iso-energy radial correlation functions of  $dI/dV$  maps at fixed energy. The x-axis denotes the energy of the maps and the y-axis the log of distance. The inset represents the same data but with a linear R axis. The black dashed line is a power law  $|E - E_c|^{-\nu}$  with  $E_c = -0.65$  eV and  $\nu = 0.75$ . **b** Radial correlations as function of energy, with E ranging from -0.8 eV to -0.43 eV. The black and red lines follow power laws of exponents -0.03 and -0.1. **c** Fractal dimension  $D_2$  as a function of energy, the inset shows a high-f zoom on multifractal spectra taken at all energies. The color codes for energy as on the main plot.

To test Eq.2, we plot on Figure 3 the dual distribution  $\tilde{\eta}^3 P(\tilde{\eta}^{-1})$  (dashed lines) which is predicted to match  $P(\tilde{\eta})$ . Clearly, the agreement is excellent in the metallic regime and relatively good for localized states ( $E > E_c = -0.65$  eV). In the high  $\tilde{\eta}$  region, we observe a systematic difference between the solid and dashed lines. We believe this latter effect to be due to the higher sensitivity of Eq.2 to experimental noise which slightly enhances the conductance of low DOS regions, namely those which dominate the dual distribution  $P(1/\tilde{\eta})$  at high  $\tilde{\eta}$ .

On Figure 3b, we plot the multifractal spectra  $f(\alpha)$  across the metal-insulator transition. Here  $2 - \alpha$  can be seen as a scaling exponent and  $f(\alpha)$  as the probability density of this scaling on a given map. When approaching the insulating phase, the spectra are broadened and shifted to the right, reaching their apex at  $\alpha_0 > 2$  [36], but they remain perfectly parabolic which is expected in our range of  $\Delta_2$  [16].

To test the symmetry relation Eq.3, we plot with dashed lines the right-hand side of Eq.3 on Figure 3b. The agreement is perfect on the entire energy range, providing a very convincing proof of the validity of Eq.3 up to the strongly localized regime and in turn demonstrating the relevance of the Weyl group symmetry hypothesis for disordered electronic systems [9]. Importantly, we note that the multifractal analysis (Eq.3) does not show the same vulnerability to experimental noise than the distribution function approach (Eq.2).

## LOCALIZED STATES

### Spectral correlations

To investigate the dispersion of localized states, we compute the energy-energy correlation function for which

criticality scalings are predicted [14, 40] (see Figure S3). Very interestingly, we report a diffuse correlation maximum around the line  $\omega = \omega_0 - E$  with  $\omega_0 = -545$  meV, ranging from the mobility edge  $E_c = -0.65$  eV up to the deeply localized regime, highlighting common features of all localized states.

### Energy-scaling of LDOS fluctuations

We now focus on the energy-scaling of LDOS fluctuations on the localized side of the transition, between the mobility edge  $E_c = -0.65$  eV and the band-edge. To allow for a fully quantitative comparison with theory and numerics, we introduce  $\eta_\Lambda(E, r) = \eta(E, r)/\eta(E_{\text{set-point}}, r)$  which accounts for fluctuations in tip-height above the sample due to the current set-point regulation of the STS spectroscopy (see Ref.[29] and SI). Note that this correction matters in the metallic regime but changes virtually nothing above  $-0.65$  eV, where localization takes place. On Figure 4 a-b, we show the mean of  $\eta_\Lambda(E)$  and its normalized standard deviation

$$\sigma(E) = \frac{\sqrt{\langle \delta \eta_\Lambda^2(E) \rangle}}{\langle \eta_\Lambda(E) \rangle_r} \quad (4)$$

Here, we mark the band-edge at  $E_{\text{edge}} = -380 \pm 50$  meV (*cf.* inset) and a high-noise region above  $-0.45$  eV, where a substantial proportion of pixels show negative tunneling conductance. Clearly, whereas the density of states decreases in a roughly linear way,  $\sigma^2$  rises very sharply on almost two decades (b).

We now shift the origin energies at the band-edge  $E_{\text{edge}} = -380 \pm 50$  meV and compute the normalized variance of  $dI/dV$  maps at energy  $E$  as a function of their distance to the gap  $|E - E_{\text{edge}}|$ . As shown on Figure 4 c, we obtain a scaling law

$$\sigma_{\text{exp}}^2(E) \sim |E - E_{\text{edge}}|^{-1.7} \quad (5)$$

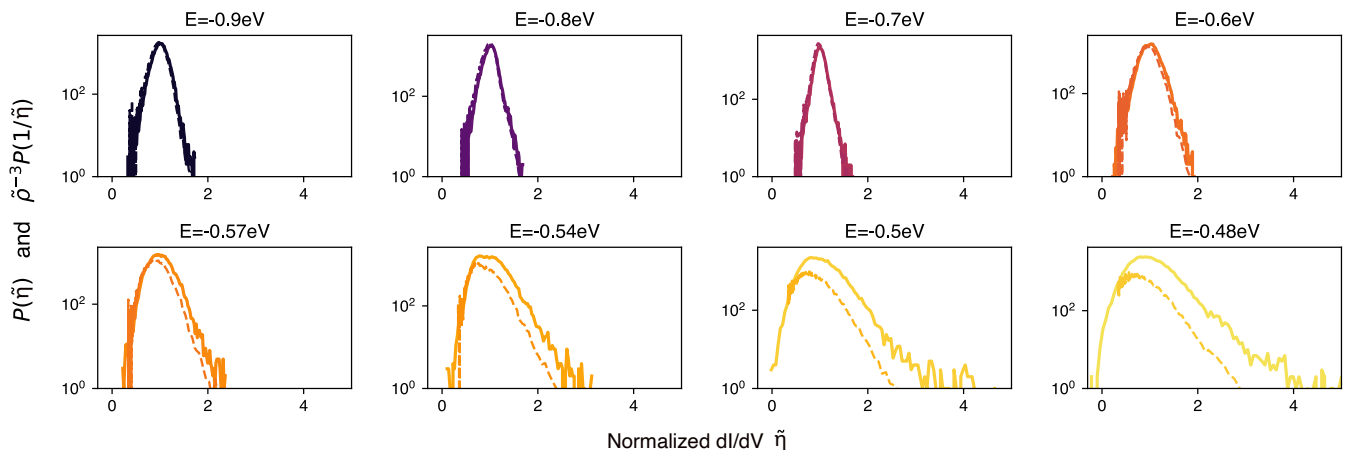
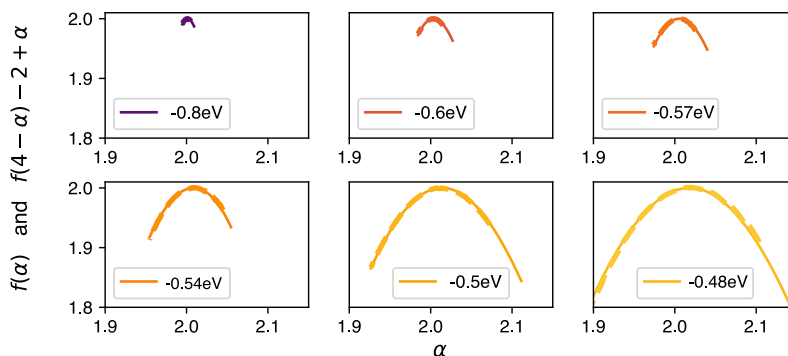
**a** Distribution functions

**b** Multifractal spectra


FIG. 3. **Distributions and multifractal analysis** **a** Solid lines denote the  $dI/dV$  distribution functions  $P(\tilde{\eta})$  of  $\tilde{\eta}(E)$  at energy  $E = \{-0.9, -0.8, -0.7, -0.6, -0.57, -0.54, -0.5, -0.48\}$  eV. Dashed lines correspond to  $\tilde{\eta}^{-3}P(1/\tilde{\eta})$ . **b** Solid lines denote the multifractal spectra  $f(\alpha)$  of  $dI/dV$  maps at energy  $E = \{-0.8, -0.6, -0.57, -0.54, -0.5, -0.48\}$  eV. Dashed lines account for  $f(4 - \alpha) - 2 + \alpha$  which were shown in Ref.[8] to coincide with  $f(\alpha)$ .

suggesting a critical behavior close to the band edge. We reproduced this measurement at the exact same position with a 6 Tesla magnetic field and found that this scaling law (Eq.5) remains strictly identical to the zero-field case. On Figure S4, we show that LDOS maps at zero and 6T are extremely similar, as expected for a Mott insulator as we can expect for an antiferromagnetic Mott-exchange insulator with an on-site Coulomb energy of about 1eV. Finally, we demonstrate a log-scaling relation between the mean and variance of LDOS maps:

$$\sigma^2 = -0.22 \log \frac{\langle \eta_{\Lambda} \rangle_r}{320 \text{pS}} \quad (6)$$

holding on more than a decade (*cf.* **d**). We are not aware of such a scaling being reported before and believe it brings a key observation on the role of density of states on Anderson transitions.

**Weak disorder analytical treatment**

As a first attempt to rationalize the power law divergence of  $\sigma(E)$ , we used a field theory model in the

weak-disorder limit and orthogonal symmetry class. We obtained closed analytical formulae for the disorder-averaged two-point spatial and spectral correlations of LDOS (see SI). In this framework, we expect  $\sigma^2$  to scale like the inverse dimensionless conductance of the layer  $g = G_{\square} h/e^2$  just like the weak localization correction to conductivity scales like  $1/g$ . In a previous study of a (superconducting) monolayer of lead on silicon, we have shown a quantitative agreement between this weak-disorder analytical model and the experimental  $\sigma^2(E)$  curve [29]. Thus, knowing the spatial and energy correlation functions of the local density of states  $\rho$ , we compute the energy-dependent variance of  $dI/dV$  maps  $\sigma^2$  and compare it to the experimental data (see SI). As shown on Figure S6-7, the model reproduces the value of  $\sigma$  close to the mobility edge as well as its divergence at the band edge. However, the exponent of the power law (Eq.5) is strongly overestimated, perhaps because the weak-disorder approximation breaks down close to the band edge.

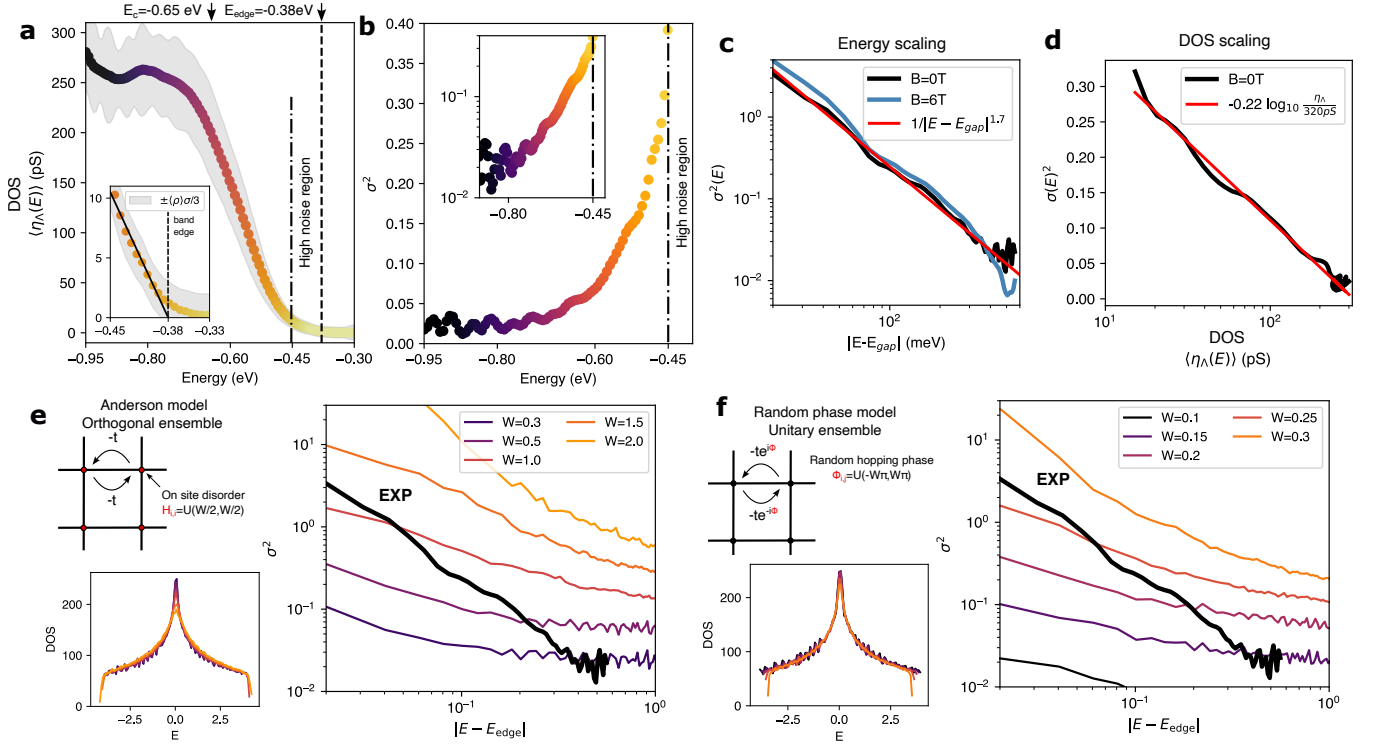


FIG. 4. **Dispersion of LDOS variance** **a** Mean normalized  $dI/dV$  spectrum  $\eta_\Lambda(E) = \langle \eta(E)/\eta(E_{\text{set-point}}) \rangle$  as a function of energy. The grey area denotes the standard deviation on the map. For  $E > -0.43$  eV, a large part of the grid's pixels have negative  $dI/dV$ , corresponding to a dominance of noise in this highly insulating region. We shall therefore focus on the  $E < -0.43$  eV region. **b** Lin-lin and lin-log plots of  $\sigma^2$ . On **c**, we shift the origin of energies to the band edge and plot  $\sigma^2$  for two different maps having different disorder realizations. We also show that adding a magnetic field of 6T does not change the scaling law. **d** Variance  $\sigma^2(E)$  versus mean  $\langle \eta_\Lambda(E) \rangle_r$  of normalized tunneling conductance. **e** Anderson model with on-site disorder and constant hopping integral  $t$ , mean density of states for various disorder levels and LDOS variance spectra as a function of energy. **f** Anderson model with random Peierls phase on each hopping integral corresponding to a random magnetic flux in each lattice cell. The phase disorder is drawn from a square distribution on  $[-W\pi, W\pi]$ .

### Scaling for extended states

Let us instead explain the scaling (5) by the divergence of the electronic wavelength  $L_E(E)$  at the band edge, an hypothesis which holds on the metallic side of the  $E_c$  and as long as the size of the map is larger than the localization length. The second moment of the LDOS  $\rho$  writes  $\langle \rho^2 \rangle / \langle \rho \rangle^2 \sim L_E^{-\Delta_2}$  and  $L_E = E^{-1/z}$  where  $z$  is the dynamical exponent of the transition [41]. For the normalized variance  $\sigma^2$ , this converts into

$$\sigma^2(E) + 1 \sim L_E^{-\Delta_2} \sim |E - E_{\text{edge}}|^{\Delta_2/z} \quad (7)$$

which yields  $\sigma^2(E) \sim E^{-\Delta_2/z} - 1$  at odds with the experimentally observed power law for Eq.5.

### Scaling for localized states

For states localized at the scale of the map, we consider that the shrinking localization length  $\xi$  close to the band edge controls the scaling [41]. Unfortunately, this

hypothesis also yields a scaling law for the second moment  $\langle \rho^2 \rangle$  and not for  $\sigma$ . For an exponentially localized wave function  $\psi$  such that  $\psi \sim e^{-|r|/\xi}/\xi^{d/2}$ , the  $q$ -th moment writes  $\int dr^d |\psi(r)|^{2q} \sim \xi^{d(1-q)}$ . For  $\sigma^2$  in 2d, we take  $q = 2$  and  $d = 2$  which gives  $\langle \rho^2 \rangle / \langle \rho \rangle^2 \sim \xi^{-2}$ . Here again the scaling for  $\sigma^2 + 1$  does not really account for our results. It is not straightforward to explain the failure of these simple scaling estimates at the band edge.

Instead, as Anderson puts it, we shall now 'resort to the indignity of numerical simulations' to explain our results [42].

### TIGHT BINDING MODELS IN VARIOUS SYMMETRY CLASSES

Let us first use the minimal model of a 2d disordered metal : the Anderson tight-binding model on a square lattice. For an on-site energy disorder, the Hamiltonian writes

$$H = -t \sum_{\langle i,j \rangle, \sigma} c_i^\dagger c_j + \sum_i (V_i - \mu) c_i^\dagger \quad (8)$$

where  $c_i^\dagger$  and  $c_i$  are respectively the creation and destruction operators on site  $i$ ,  $t$  is the hopping integral,  $V_i$  the disorder drawn from a uniform distribution on  $[-W/2, W/2]$  and  $\mu$  the electronic chemical potential. We obtain the eigenstates of  $H$  by an exact diagonalization on a  $100 \times 100$  lattice and construct maps of the local density of states by summing eigenstates in an energy window corresponding to the spectral width of our STM measurement. The normalized variance  $\sigma(E)^2$ , defined exactly as in Eq.4 is plotted on Figure 4e – the origin of energies is taken as the lowest eigenvalue – and is compatible with a scaling law

$$\sigma_{\text{orth}}^2(E) \sim |E - E_{\text{edge}}|^{-2/3} \quad (9)$$

Although the exponent is not exactly the same as in experiments ( $-1.7$ ), the qualitative trend is very similar.

### Unitary symmetry class

Let us not forget here that our tin monolayer is a strongly correlated material [5, 6]. As a consequence, we do not expect it to be properly described by a non-interacting Anderson model. As a full account for Coulombic interactions in large disordered lattices is out of reach for current numerical methods, we instead focus on the symmetry class of the Hamiltonian in the sense of the random matrix theory [16]. As a first attempt to consider the role of electronic symmetry, the presence of Mott-like correlations and hints of a magnetic order lead us to consider a possible breaking of time-reversal symmetry leading us from the orthogonal to the unitary symmetry class. We write a minimalistic tight-binding model in which a random magnetic field breaks time-reversal symmetry. Effectively, we change the nature of disorder by removing the on-site terms  $V_i$  and replacing them with a random Peirls phase on each hopping integral ( $te^{i\phi_i}$ ) where  $\phi$  follows a square distribution on  $[-W\pi, W\pi]$ . Note that this disorder corresponds to a random magnetic field in each lattice cell.

The normalized variance  $\sigma(E)^2$  is plotted on Figure 4f for several disorder levels. Firstly, like the Anderson model on e, this random-phase model qualitatively reproduces the divergence in  $\sigma^2$ . But more interestingly, the unitary-class model improves on the orthogonal Anderson model, especially very close to the band-edge. Although the agreement is not perfect, this shows that the nature of disorder – on-site potential or random phase –

influences Anderson localization patterns, as previously reported in a number of theoretical and numerical works [16, 43]. On the numerical side, the Anderson-Hubbard model, coupling on-site repulsion to disorder, seems the most straightforward extension of our work [44, 45]. Fractal and scaling analysis in the symplectic class would also be very valuable. Finally, we remark that critical scalings are measured not only in LDOS maps but also in transport coefficients, for instance in the universal conductance fluctuations [31]. In this way, our inference of electronic symmetries from electronic fluctuations could be generalized to mesoscopic circuits in general instead of being restricted to very demanding tunneling spectroscopy maps.

### CONCLUSION

We evidence the metal-insulator transition close to the valence band-edge of a strongly correlated 2d material, the  $\sqrt{3} \times \sqrt{3}$  phase of tin on silicon. From LDOS spatial correlations, we find an apparent mobility edge with a critical exponent  $\nu = 0.75$ . The symmetry of multifractal spectra across the transition and in excellent agreement with the theory, based on the Weyl-group symmetry of non-linear  $\sigma$  models. Finally, we report an energy scaling for the LDOS variance close to the band-edge  $\sigma^2 \sim |E - E_{\text{edge}}|^{-1.7}$ . We find that Anderson models reproduce qualitatively the strong rise in LDOS relative variance  $\sigma$ . A key observation is that a unitary-class model – where a random magnetic fields breaks time-reversal symmetry – is closer to the experimental results than the standard orthogonal Anderson model.

Although the understanding of localization for correlated electronic systems of various symmetries is still an open field, our results provide a unifying picture by bridging together many key results in a consistent picture on a single model material. The observation of multifractal scalings in the universal conductance fluctuations for high-mobility graphene [31] brings a very promising perspective for an extension of our methodology to transport experiments, beyond the very demanding STM spectroscopy.

### Acknowledgements

M.L thanks Igor Burmistrov for countless enlightening discussions.

- 
- [1] I. Burmistrov, I. Gornyi, and A. Mirlin, Enhancement of the critical temperature of superconductors by anderson localization, *Physical review letters* **108**, 017002 (2012).  
 [2] B. Sacépé, M. Feigel'man, and T. M. Klapwijk, Quantum breakdown of superconductivity in low-dimensional

- materials, *Nature Physics* **16**, 734 (2020).  
 [3] D. A. Abanin, E. Altman, I. Bloch, and M. Serbyn, Colloquium: Many-body localization, thermalization, and entanglement, *Reviews of Modern Physics* **91**, 021001 (2019).

- [4] S. Modesti, L. Petaccia, G. Ceballos, I. Vobornik, G. Panaccione, G. Rossi, L. Ottaviano, R. Larciprete, S. Lizzit, and A. Goldoni, Insulating ground state of sn/si (111)-(3×3) r 30, *Physical review letters* **98**, 126401 (2007).
- [5] F. Ming, S. Johnston, D. Mulugeta, T. S. Smith, P. Vilmercati, G. Lee, T. A. Maier, P. C. Snijders, and H. H. Weitering, Realization of a hole-doped mott insulator on a triangular silicon lattice, *Physical Review Letters* **119**, 266802 (2017).
- [6] M. Torkzadeh, A. Thakur, C. Tresca, M. Lizée, M. Hervé, F. Debontridder, P. David, G. Profeta, T. Cea, T. Cren, M. Calandra, and C. Brun, Two-dimensional antiferromagnetic and large-gap insulating ground state of the correlated  $\sqrt{3} \times \sqrt{3}$  r30-sn/si(111) single atomic layer, In preparation (2025).
- [7] A. D. Mirlin and Y. V. Fyodorov, Distribution of local densities of states, order parameter function, and critical behavior near the anderson transition, *Physical review letters* **72**, 526 (1994).
- [8] A. D. Mirlin, Y. V. Fyodorov, A. Mildenerger, and F. Evers, Exact relations between multifractal exponents at the anderson transition, *Phys. Rev. Lett.* **97**, 046803 (2006).
- [9] I. Gruzberg, A. Ludwig, A. Mirlin, and M. Zirnbauer, Symmetries of multifractal spectra and field theories of anderson localization, *Physical Review Letters* **107**, 086403 (2011).
- [10] B. Sacépé, C. Chapelier, T. Baturina, V. Vinokur, M. Baklanov, and M. Sanquer, Disorder-induced inhomogeneities of the superconducting state close to the superconductor-insulator transition, *Physical review letters* **101**, 157006 (2008).
- [11] M. Feigel'Man, L. Ioffe, V. Kravtsov, and E. Cuevas, Fractal superconductivity near localization threshold, *Annals of Physics* **325**, 1390 (2010).
- [12] T. Charpentier, D. Perconte, S. Léger, K. R. Amin, F. Blondelle, F. Gay, O. Buisson, L. Ioffe, A. Khvalyuk, I. Poboiko, *et al.*, First-order quantum breakdown of superconductivity in an amorphous superconductor, *Nature Physics* , 1 (2025).
- [13] D. Belitz and T. Kirkpatrick, The anderson-mott transition, *Reviews of modern physics* **66**, 261 (1994).
- [14] I. Burmistrov, I. Gornyi, and A. Mirlin, Multifractality at anderson transitions with coulomb interaction, *Physical Review Letters* **111**, 066601 (2013).
- [15] C. Groth, M. Wimmer, A. Akhmerov, J. Tworzydło, and C. Beenakker, Theory of the topological anderson insulator, *Physical review letters* **103**, 196805 (2009).
- [16] F. Evers and A. D. Mirlin, Anderson transitions, *Reviews of Modern Physics* **80**, 1355 (2008).
- [17] K. Hashimoto, C. Sohrmann, J. Wiebe, T. Inaoka, F. Meier, Y. Hirayama, R. A. Römer, R. Wiesendanger, and M. Morgenstern, Quantum hall transition in real space: from localized to extended states, *Physical Review Letters* **101**, 256802 (2008).
- [18] A. Richardella, P. Roushan, S. Mack, B. Zhou, D. A. Huse, D. D. Awschalom, and A. Yazdani, Visualizing critical correlations near the metal-insulator transition in  $\text{Ga}_1-x\text{Mn}_x\text{As}$ , *science* **327**, 665 (2010).
- [19] B. Jäck, F. Zinser, E. J. König, S. N. Wissing, A. B. Schmidt, M. Donath, K. Kern, and C. R. Ast, Visualizing the multifractal wave functions of a disordered two-dimensional electron gas, *Physical Review Research* **3**, 013022 (2021).
- [20] B. G. Shin, J.-H. Park, J. Kong, and S. J. Jung, Characterizing critical behavior and band tails on the metal-insulator transition in structurally disordered two-dimensional semiconductors: Autocorrelation and multifractal analysis, *Physical Review Research* **5**, 043029 (2023).
- [21] B. G. Shin, J.-H. Park, J.-Y. Juo, J. Kong, and S. J. Jung, Structural-disorder-driven critical quantum fluctuation and localization in two-dimensional semiconductors, *Nature Communications* **14**, 2283 (2023).
- [22] A. Ghosal, M. Randeria, and N. Trivedi, Inhomogeneous pairing in highly disordered s-wave superconductors, *Physical Review B* **65**, 014501 (2001).
- [23] C. Carbillet, S. Caprara, M. Grilli, C. Brun, T. Cren, F. Debontridder, B. Vignolle, W. Tabis, D. Demaille, L. Largeau, *et al.*, Confinement of superconducting fluctuations due to emergent electronic inhomogeneities, *Physical Review B* **93**, 144509 (2016).
- [24] C. Carbillet, V. Cherkez, M. Skvortsov, M. Feigel'Man, F. Debontridder, L. Ioffe, V. Stolyarov, K. Ilin, M. Siegel, D. Roditchev, *et al.*, Spectroscopic evidence for strong correlations between local superconducting gap and local altshuler-aronov density of states suppression in ultrathin nbn films, *Physical Review B* **102**, 024504 (2020).
- [25] E. Andriyakhina and I. Burmistrov, Multifractally-enhanced superconductivity in two-dimensional systems with spin-orbit coupling, *Journal of Experimental and Theoretical Physics* **135**, 484 (2022).
- [26] C. Brun, T. Cren, V. Cherkez, F. Debontridder, S. Pons, D. Fokin, M. Tringides, S. Bozhko, L. Ioffe, B. Altshuler, *et al.*, Remarkable effects of disorder on superconductivity of single atomic layers of lead on silicon, *Nature Physics* **10**, 444 (2014).
- [27] C. Rubio-Verdú, A. M. García-García, H. Ryu, D.-J. Choi, J. Zaldívar, S. Tang, B. Fan, Z.-X. Shen, S.-K. Mo, J. I. Pascual, *et al.*, Visualization of multifractal superconductivity in a two-dimensional transition metal dichalcogenide in the weak-disorder regime, *Nano letters* **20**, 5111 (2020).
- [28] M. Stosiek, F. Evers, and I. Burmistrov, Multifractal correlations of the local density of states in dirty superconducting films, *Physical Review Research* **3**, L042016 (2021).
- [29] M. Lizée, M. Stosiek, I. Burmistrov, T. Cren, and C. Brun, Local density of states fluctuations in a two-dimensional superconductor as a probe of quantum diffusion, *Physical Review B* **107**, 174508 (2023).
- [30] F. Ming, X. Wu, C. Chen, K. D. Wang, P. Mai, T. A. Maier, J. Stroockoz, J. Venderbos, C. González, J. Ortega, *et al.*, Evidence for chiral superconductivity on a silicon surface, *Nature Physics* **19**, 500 (2023).
- [31] K. R. Amin, S. S. Ray, N. Pal, R. Pandit, and A. Bid, Exotic multifractal conductance fluctuations in graphene, *Communications Physics* **1**, 1 (2018).
- [32] A. Odobescu, A. Maizlakh, N. Fedotov, and S. Zaitsev-Zotov, Electronic correlation effects and coulomb gap in the si (111)-(3×3)-sn surface, *Physical Review B* **95**, 195151 (2017).
- [33] S. Yi, F. Ming, Y.-T. Huang, T. S. Smith, X. Peng, W. Tu, D. Mulugeta, R. D. Diehl, P. C. Snijders, J.-H. Cho, *et al.*, Atomic and electronic structure of doped si (111)( $2 \times 3 \times 2 \times 3$ ) r 30-sn interfaces, *Physical Review B* **97**, 195402 (2018).



- [34] M. Jager, C. Brand, A. Weber, M. Fanciulli, J. Dil, H. Pfnür, and C. Tegenkamp,  $\alpha$ -sn phase on si (111): Spin texture of a two-dimensional mott state, *Physical Review B* **98**, 165422 (2018).
- [35] K. Zhao, H. Lin, X. Xiao, W. Huang, W. Yao, M. Yan, Y. Xing, Q. Zhang, Z.-X. Li, S. Hoshino, *et al.*, Disorder-induced multifractal superconductivity in monolayer niobium dichalcogenides, *Nature Physics* **15**, 904 (2019).
- [36] M. Schreiber and H. Grussbach, Multifractal wave functions at the anderson transition, *Physical Review Letters* **67**, 607 (1991).
- [37] A. Chhabra and R. V. Jensen, Direct determination of the  $f(\alpha)$  singularity spectrum, *Physical Review Letters* **62**, 1327 (1989).
- [38] I. A. Gruzberg, A. Mirlin, and M. Zirnbauer, Classification and symmetry properties of scaling dimensions at anderson transitions, *Physical Review B—Condensed Matter and Materials Physics* **87**, 125144 (2013).
- [39] F. Evers, A. Mildenerger, and A. Mirlin, Multifractality at the quantum hall transition: Beyond the parabolic paradigm, *Physical Review Letters* **101**, 116803 (2008).
- [40] E. Cuevas and V. E. Kravtsov, Two-eigenfunction correlation in a multifractal metal and insulator, *Physical Review B—Condensed Matter and Materials Physics* **76**, 235119 (2007).
- [41] I. Burmistrov, I. Gornyi, and A. Mirlin, Tunneling into the localized phase near anderson transitions with coulomb interaction, *Physical Review B* **89**, 035430 (2014).
- [42] P. W. Anderson, Local moments and localized states (nobel lecture), *Usp. Fiz. Nauk* **127**, 19 (1979).
- [43] L. Ujfalusi and I. Varga, Finite-size scaling and multifractality at the anderson transition for the three wigner-dyson symmetry classes in three dimensions, *Physical Review B* **91**, 184206 (2015).
- [44] H. Shinaoka and M. Imada, Single-particle excitations under coexisting electron correlation and disorder: A numerical study of the anderson–hubbard model, *Journal of the Physical Society of Japan* **78**, 094708 (2009).
- [45] H. Shinaoka and M. Imada, Soft hubbard gaps in disordered itinerant models with short-range interaction, *Physical Review Letters* **102**, 016404 (2009).